life

MDPI

Article

Neoadjuvant Chemotherapy Preserves Tumor Cell-Intrinsic Chemosensitivity but Reshapes the Immune Microenvironment in High-Grade Serous Ovarian Cancer

Tongle Zhang [1,2,†], Luyang Zhao [2,†], Yawen Wu [2,†], Li'an Li [2], Zhifeng Yan [2], Qingzhi Zhai [2], Mingxia Li [2], Yue Wang [2], Xiaoyu Fu [2], Mingyang Wang [2], Nan Wang [2], Mengyu Chen [1,2], Xinyu Wang [1,2], Shujie Liao [2], Yuanguang Meng [1,2,*] and Mingxia Ye [1,2,*]

[1] School of Medicine, Nankai University, Tianjin 300071, China; nku_ztl@163.com (T.Z.)
[2] Senior Department of Obstetrics and Gynecology, Chinese PLA General Hospital, Beijing 100853, China
* Correspondence: meng6512@vip.sina.com (Y.M.); ymx298013@126.com (M.Y.)
† These authors contributed equally to this work.

Abstract

Whether neoadjuvant chemotherapy (NACT) induces chemoresistance in high-grade serous ovarian cancer (HGSOC) remains controversial, with conflicting clinical evidence regarding platinum resistance following NACT and interval debulking surgery (IDS). To elucidate this paradigm, the present study was designed to systematically interrogate the molecular and cellular underpinnings of NACT-driven resistance, and to comprehensively characterize the dynamic genomic alterations and tumor microenvironment (TME) remodeling that occur over the course of NACT administration. We prospectively established paired patient-derived organoids (PDOs) from 14 HGSOC patients before and after NACT, integrated with whole-exome sequencing (WES) and RNA sequencing of matched tumor specimens (PDO cohort: $n = 13$; genomic/transcriptomic cohort: $n = 11$), and correlated findings with clinical outcomes, specifically the time to tumor progression (TTP) and chemotherapy response. HGSOC-derived PDOs highly recapitulated the histological and genomic features of parental tumors. Functional chemosensitivity profiling revealed that PDO drug responses remained largely unchanged following NACT, particularly among strictly site-matched paired samples, with more cases exhibiting increased rather than decreased platinum sensitivity. No significant divergence in tumor mutational burden (TMB), intratumoral heterogeneity (ITH), apolipoprotein B mRNA-editing enzyme catalytic-polypeptide (APOBEC) score, homologous recombination deficiency (HRD) score, and Signature 3 and dN/dS ratio was observed between paired pre- and post-NACT specimens. In contrast, post-NACT tumors exhibited significantly enhanced infiltration of $CD8^+$ T cells, natural killer (NK) cells, activated NK cells, B lineage, cytotoxic lymphocytes, myeloid dendritic cells and higher CYT score. Integrative analysis revealed preliminary associations between PDO-defined chemosensitivity and clinical chemotherapy response score, as well as TTP. Our exploratory study suggests that NACT largely preserves tumor cell-intrinsic chemosensitivity but may reshape the tumor microenvironment toward a more immunogenic state. These findings provide a rationale for future investigation into combining NACT with immune checkpoint blockade. However, given the limited sample size, PDO-based functional testing requires further prospective validation before it can be considered a predictive tool for personalized treatment selection.

Keywords: high-grade serous ovarian cancer; neoadjuvant chemotherapy; patient-derived tumor organoids; chemoresistance; tumor microenvironment

Check for updates

Academic Editors: Ahmed Lasfar, Katalin Prokai-Tatrai and Pranela Rameshwar

Received: 12 October 2026
Revised: 16 November 2026
Accepted: 26 November 2026
Published: 28 November 2026

Copyright: © 2026 by the authors. Licensee MDPI, Basel, Switzerland. This article is an open access article distributed under the terms and conditions of the Creative Commons Attribution (CC BY) license.

1. Introduction

Ovarian cancer remains the most lethal gynecological malignancy worldwide, accounting for approximately 206,839 deaths annually [1]. High-grade serous ovarian cancer (HGSOC) represents the most common and aggressive subtype of epithelial ovarian cancer (EOC) [2], characterized by late-stage presentation, extensive peritoneal dissemination, and 10-year survival rate below 30% [3,4]. The standard treatment for advanced EOC is primary debulking surgery (PDS) followed by platinum-based adjuvant chemotherapy [5]. However, for patients who are not suitable for PDS or diagnosed with unresectable diseases, neoadjuvant chemotherapy (NACT) followed by interval debulking surgery (IDS) has been the recommended as the alternative treatment option [5]. Over the past decade, the therapeutic landscape for advanced HGSOC has progressively shifted toward more frequent use of NACT-IDS, with approximately 40% of advanced HGSOC patients now receiving NACT as their initial treatment, although this proportion varies considerably across geographic regions and institutional practices [6]. Therefore, therapeutic paradigm for advanced HGSOC patients has shifted from a focus on PDS followed by adjuvant chemotherapy to more frequent use of NACT followed by IDS in recent years. The clinical rationale for NACT lies in its capacity to facilitate complete macroscopic resection at IDS [7,8] and to reduce perioperative morbidity and mortality compared with PDS [9].

Despite these surgical advantages, the long-term oncological benefit of NACT-IDS remains contentious. Accumulating retrospective evidence has raised the possibility that NACT may promote chemoresistance, with several studies reporting higher rates of platinum-resistant recurrence in NACT-IDS cohorts compared with PDS counterparts [10]. Mechanistically, NACT-associated chemoresistance has been proposed to arise through Darwinian selection of pre-existing resistant subclones, chemotherapy-induced mutagenesis, and epigenetic reprogramming [11]. Specific molecular alterations, including TP53 mutations [12,13], BRCA1/2 reversion mutations [14,15], and changes in homologous recombination deficiency (HRD) status [16], have been implicated in post-NACT platinum resistance. Conversely, other investigations have reported no significant increase in platinum resistance following NACT [17,18], and recent paired genomic analyses have demonstrated remarkable stability of driver mutations and overall mutational burden between pre- and post-NACT specimens [19]. This apparent discrepancy between clinical observations and molecular evidence highlights a critical knowledge gap: whether NACT genuinely reprograms HGSOC cells toward an intrinsically chemoresistant state, or whether post-NACT chemoresistance reflects non-cell-autonomous mechanisms mediated by the tumor microenvironment (TME), remains unresolved.

Resolving this controversy has been hampered by the limitations of existing experimental approaches. Conventional two-dimensional cell lines fail to recapitulate intratumoral heterogeneity and the three-dimensional architecture critical for modeling drug response [20], while bulk tissue sequencing alone cannot disentangle tumor cell-intrinsic chemosensitivity from microenvironment-mediated effects. Patient-derived organoids (PDOs)—three-dimensional culture systems that faithfully preserve the histological, genomic, and functional characteristics of parental tumors—have emerged as a powerful preclinical platform for investigating tumor biology and predicting therapeutic response [21]. In HGSOC, PDOs have been shown to maintain the genomic landscape of primary tumors and predict clinical responses to platinum-based chemotherapy and Poly (ADP-ribose) polymerase (PARP) inhibitors with high fidelity [22]. Moreover, integrating PDO-based functional drug sensitivity assays with paired multi-omics profiling of primary tumors provides a unique opportunity to dissect the relative contributions of tumor cell-intrinsic and TME-mediated mechanisms to NACT-associated chemoresistance—an approach that has yet to be systematically applied to paired pre- and post-NACT HGSOC specimens.

In the present study, we sought to address the longstanding controversy surrounding NACT-induced chemoresistance in HGSOC through an integrative, multidimensional analysis of paired pre- and post-NACT specimens. We tested three interrelated hypotheses: (i) whether NACT alters tumor cell-intrinsic chemosensitivity, as assessed by paired PDO drug response assays; (ii) whether NACT drives significant genomic evolution, including changes in tumor mutational burden (TMB), intratumoral heterogeneity (ITH), HRD score, and mutational signatures; and (iii) whether NACT remodels the immune contexture of the TME, thereby creating a therapeutic window for combinatorial immunotherapy. By integrating PDO-based functional assays with whole-exome and transcriptomic sequencing of paired clinical specimens, our study aims to provide convergent evidence on the biological consequences of NACT in HGSOC and to inform rational treatment strategies for patients ineligible for primary debulking surgery.

2. Materials and Methods

2.1. Patient Enrollment and Specimen Collection

This study was approved by the Ethical Committee of the Chinese People's Liberation Army (PLA) General Hospital (approval No. S2021-520-01), and written informed consent was obtained from all participants. Patients diagnosed with HGSOC who were scheduled to receive NACT followed by IDS between 2021 and 2023 were prospectively enrolled. Pre-NACT tumor specimens were obtained via laparoscopic biopsy or diagnostic aspiration at the time of initial diagnosis, and post-NACT specimens were collected during IDS. Specimens were procured from primary ovarian masses, omental or peritoneal metastases, and malignant ascites or pleural effusions. Fresh tissue was immediately transported to the laboratory in ice-cold transport medium for organoid establishment, with parallel specimens preserved for histopathological examination, snap-frozen for nucleic acid extraction, or fixed in formalin for immunohistochemistry.

Comprehensive clinical and treatment data were retrospectively extracted from the electronic medical records. For all enrolled patients, the specific NACT regimens (primarily Nab-paclitaxel + Carboplatin or Liposomal paclitaxel + Carboplatin), the number of treatment cycles before IDS (ranging from 1 to 4 cycles), and the interval between the completion of NACT and sample collection (ranging from 23 to 37 days, median: 28 days) were documented. Detailed NACT regimens, cycle numbers, and sampling intervals for each patient are summarized in Table 1.

Time to tumor progression (TTP) was calculated from the date of the last cycle of adjuvant chemotherapy (or the date of IDS, if no adjuvant chemotherapy was given) to the date of documented disease progression or recurrence. Platinum resistance was defined clinically according to standard criteria (progression within 6 months of platinum-based therapy), which was distinguished from the in vitro PDO chemosensitivity (IC_{50}) evaluated in this study.

Table 1. Patient and specimen characteristics.

Patient	Age	FIGO Stage	NACT Regimen	NACT Cycles	Interval (Days)	PDO Sample ID	WES/RNA-Seq Sample ID
P1	73	IIIC	Nab-paclitaxel + Carboplatin	3	33	P1_Ova_pre, P1_Per_pre, P1_Asc_pre, P1_Ome_pre, P1_Ome_post	P1_Ova_pre, P1_Ova_post
P2	78	IIIB	Nab-paclitaxel + Carboplatin	2	34	P2_Ova_pre	P2_Ova_pre, P2_Ova_post
P3	68	IVB	Liposomal paclitaxel + Carboplatin	3	32	P3_Ova_pre, P3_Ome_pre	P3_Ova_pre, P3_Ome_pre, P3_Ova_post, P3_Ome_post
P4	67	IIIC	Liposomal paclitaxel + Carboplatin	3	37	P4_Ome_pre	P4_Ome_pre, P4_Ome_post
P5	48	IVB	Liposomal paclitaxel + Carboplatin	4	23	P5_Per_pre	P5_Ova_pre, P5_Ova_post
P6	49	IIIC	Nab-paclitaxel + Carboplatin	2	33	P6_Ova_pre	P6_Ova_pre, P6_Ova_post
P7	45	IVB	Nab-paclitaxel + Carboplatin	3	33	P7_Ova_pre, P7_Per_pre, P7_Ome_pre, P7_Ova_post	P7_Ome_pre, P7_Ova_pre, P7_Ome_post, P7_Ova_post
P8	66	IIIC	Liposomal paclitaxel + Carboplatin	2	39	N/A (Culture failed)	P8_Ova_pre, P8_Ova_post
P9	55	IIIC	Liposomal paclitaxel + Carboplatin	2	25	P9_Ome_pre	P9_Ova_pre, P9_Ova_post
P10	40	IVB	Liposomal paclitaxel + Carboplatin	2	26	P10_Ova_pre, P10_Per_pre, P10_Ome_pre, P10_Ova_post, P10_Per_post, P10_Ome_post	P10_Ova_pre, P10_Ova_post
P11	60	IIIB	Nab-paclitaxel + Carboplatin	3	26	P11_Ova_pre, P11_Asc_pre, P11_Asc_post, P11_Ome_post	P11_Ova_pre, P11_Ova_post
P12	51	IVB	Paclitaxel + Intraperitoneal Cisplatin	1	27	P12_Asc_pre, P12_Per_post	N/A
P13	70	IVA	Nab-paclitaxel + Carboplatin	3	27	P13_Ple_pre, P13_Ova_post	N/A
P14	65	IIIC	Liposomal paclitaxel + Carboplatin	3	28	P14_Ova_pre, P14_Asc_pre, P14_Ome_post	N/A

Organoids nomenclature is based on corresponding patient number, anatomical site of origin, and chemotherapy exposure status at collection. Note: A total of 14 HGSOC patients (P1–P14) were prospectively enrolled. Patient 8 (P8) was included in the genomic and transcriptomic analyses (P1–P11) but was excluded from the PDO drug sensitivity analyses due to failed organoid culture. Conversely, Patients 12–14 (P12–P14) had successful PDO assays but lacked paired RNA-seq and WES data. Abbreviations: Ova, ovarian. Per, peritoneum. Ome, omentum. Asc, ascitic effusion. Ple, pleural effusion.

2.2. PDO Establishment and Culture

Fresh tumor tissues were collected immediately after surgery. Non-necrotic areas with solid or papillary growth were carefully selected and minced into approximately 1 mm^3 fragments. The fragments were washed with cold HBSS (BasalMedia, Shanghai, China) and enzymatically digested using tumor tissue dissociation solution (Accuroid, Guangzhou, China) (30–120 min) to obtain single cells. The suspension was repeatedly triturated and passed through a 70-μm cell strainer. Following centrifugation, the cell pellet was resuspended in Matrigel (Corning, NY, USA) at a ratio of 1:2 (v/v) and seeded upside down into pre-warmed 6-well culture plates (Youlai, Hangzhou, China). Following Matrigel solidification at 37 °C for 20–30 min, ovarian cancer organoid medium was added. The medium was changed every 2–3 days, and organoids were passaged every 4–7 days based on morphological viability criteria.

2.3. Histological Analysis and Immunohistochemistry

Hematoxylin and eosin (H&E) staining and immunohistochemistry (IHC) were performed on formalin-fixed, paraffin-embedded (FFPE) sections of patient tumors and corresponding organoids. Primary antibodies against p53, PAX8, WT1, CK7 (Proteintech, Wuhan, China), and HER2 (CST, Danvers, MA, USA) were applied at manufacturer-recommended dilutions, followed by avidin-biotin peroxidase detection. Images were captured using an Optec microscope (Optec, Chongqing, China). Organoid histology was independently reviewed by two pathologists.

2.4. Whole-Exome Sequencing (WES)

Tumor DNA were extracted using the QIAamp DNA FFPE Tissue Kit (56404, Qiagen, Hilden, Germany) from formalin-fixed paraffin-embedded tissues or using the TIANamp Genomic DNA Kit (DP304, TIANGEN, Beijing, China) from fresh tumor tissues. Matched normal DNA were extracted using the TIANamp Genomic DNA Kit (DP304, TIANGEN, Beijing, China) from paired blood samples. Agilent SureSelectXT Human All Exon V6 Kit (5190-8864, Agilent Technologies, Santa Clara, CA, USA) was used to capture all exon target sequences, and then DNA libraries were constructed with KAPA Library Preparation Kit (Kapa Biosystems Inc., Wilmington, MA, USA). Briefly, genomic DNA was fragmented, end-repaired, adenylated at the 3′ ends, end-connected, amplified, purified, and size-selected in the process of library construction, then was sequenced on the Illumina NovaSeq6000 platform (Illumina Inc., San Diego, CA, USA).

2.5. Organoid Drug Sensitivity Assay

Treatment of anticancer drugs and sensitivity tests were performed as previously described by our group [23] with modifications. Briefly, organoids (40–100 μm in diameter) cultured for 1–2 weeks were collected and dissociated, then mixed with Matrigel at a 1:1 ratio and seeded into 384-well plates (Youlai, Hangzhou, China) at approximately 2000 cells per well with 5–6 technical replicates per condition. Following a 48 h culture period, the organoids were treated with serial half-log dilutions of carboplatin, paclitaxel–carboplatin (TC), adriamycin–carboplatin, docetaxel–carboplatin, epirubicin, gemcitabine, etoposide, niraparib, or olaparib. Following a 96 h drug incubation, cell viability was evaluated using 3D CellTiter-Glo (Promega, Madison, WI, USA). The plates were subjected to agitation for a duration of 30 min at room temperature before measuring luminescence. The luminescence signal was normalized to the untreated control group (defined as 100% viability) to calculate the relative cell viability. IC_{50} values were determined utilizing GraphPad Prism 9.0 software (GraphPad Software, San Diego, CA, USA). To classify PDOs as chemotherapy-sensitive or resistant, an IC_{50} cut-off threshold of 1.6 was applied. This specific threshold was not

arbitrarily chosen; rather, it was established based on our laboratory's extensive historical cohort of ovarian cancer PDOs, where in vitro IC_{50} values were directly correlated with patients' clinical platinum responses to define the most accurate discriminating cut-off.

2.6. Data Extraction for Clinical Correlation

To account for intra-tumor spatial heterogeneity, baseline PDO chemosensitivity was selected using two complementary strategies prior to survival analysis. First, only PDOs derived from pre-NACT lesions were included. Second, for drug selection, carboplatin IC_{50} values were prioritized; if unavailable, paclitaxel–carboplatin (TC) IC_{50} values were used. Based on these criteria, the two strategies were applied as follows: (1) Primary-site prioritization: the value from the primary ovarian lesion was prioritized, followed by omental/peritoneal metastases; (2) Most-resistant solid lesion prioritization: the highest IC_{50} among all available solid lesions was selected to capture the most drug-resistant subclone, excluding ascites/pleural effusion to avoid non-solid microenvironment confounding. Patients were then stratified into sensitive and resistant groups based on the median IC_{50} of the respective cohort.

2.7. Somatic Mutation Calling and Filtering

Somatic SNVs and InDels were called using GATK MuTect2 (version 4.1), followed by variant-level filtering using GATK FilterMutectCalls. Only variants with a FILTER status of "PASS" in the resulting VCF files were retained for downstream analysis. The retained variants were subsequently annotated using ANNOVAR (version 2016-02-01). Further filtering criteria included retaining variants located in exonic, exonic;splicing, or splicing regions, excluding synonymous SNVs and variants with unknown functional annotations, and retaining variants with a tumor variant allele frequency (VAF) of ≥2%.

2.8. Apolipoprotein B mRNA-Editing Enzyme Catalytic-Polypeptide (APOBEC) Enrichment Score and dN/dS Ratio Analysis

APOBEC could deaminate cytidines predominantly in a 'TCW' motif (W = A or T). For each tumor, the APOBEC mutagenesis enrichment score was analyzed on the basis of C > T mutations occurring in 'TCW' motifs as described by Roberts and colleagues with 'P-MACD' R packages (version 1.0.0) [24]. dN/dS ratios for missense and nonsense mutations were estimated by dNdScv R package [25] to quantify selection in cancer and somatic evolution.

2.9. Tumor Mutational Burden (TMB), Intratumoral Heterogeneity (ITH), Homologous Recombination Deficiency (HRD) and Somatic Mutational Signature Analysis

TMB was estimated with the number of somatic, coding, base substitution, and indel mutations per megabase of gene region targeted (mutations/Mb). The ITH was evaluated by mutant-allele tumor heterogeneity algorithm [26] and HRD score was calculated with the 'scarHRD' R package [27]. Decomposition of mutational signatures was performed using the R package 'deconstructSigs' (version 1.8.0) [28], based on the set of 30 COSMIC mutational signatures (https://cancer.sanger.ac.uk/signatures/signatures_v2/, accessed on 26 November 2026) for all these samples, which were analyzed on the basis of the single nucleotide variants (SNVs) and their sequence context, considering the immediately flanking 5′ and 3′ nucleotides. Mutational signatures with ≥ 0.08 weight of each case were considered to have substantial contribution to the mutational landscape of a sample.

2.10. RNA Sequencing and Gene Expression

Total RNA was extracted from fresh or FFPE tumor tissues using TRIzol® Reagent (#15596018, Invitrogen, Waltham, MA, USA) or RNeasy FFPE Kit (#73504, Qiagen, Hilden,

Germany), respectively. RNA libraries were constructed using NEBNext® Ultra™ RNA Library Prep Kits (#E7770/#E7420, NEB, Ipswich, MA, USA) and sequenced on the Illumina NovaSeq 6000 platform (Illumina Inc., San Diego, CA, USA). Raw reads were filtered to remove adapter sequences, reads with >5% Ns, and reads with >15% low-quality bases ($Q \leq 19$). Clean reads were aligned to the hg19 reference genome using Tophat2 (v2.0.10)/Bowtie2 (v2.2.4), and gene expression was quantified as FPKM or TPM using Cufflinks (v2.2.1).

2.11. Assessment of Immune Infiltration

Immune infiltration of different cell subtypes in each tumor tissue were estimated by two bioinformatics algorithms, including CIBERSORT [29] and MCP-counter (version 1.1.0, default parameters) [30]. Additionally, the immune cytolytic activity (named as 'CYT score') for each sample was calculated as the geometric mean based on the expression (expressed in TPM) of two genes granzyme A (GZMA) and perforin (PRF1) [31].

2.12. Gene Set Enrichment Analysis (GSEA)

GSEABase (version 1.58.0, default parameters) was used to identify the significant enriched pathways between two groups based on fold changes of gene expression. Enrichment results with $|NES| > 1$, nominal p-value < 0.05, and false discovery rate (FDR) q-value < 0.25 were considered statistically significant.

2.13. Graphics

Gene mutation landscape was plotted with the R package 'ComplexHeatmap' (version 2.12.1). The histogram of mutational signatures were plotted with the R package 'ggplot2' (version 3.4.1). KEGG pathway enrichment results were also visualized by the R package 'ggplot2' (version 3.4.1). All the scatter diagrams and histograms were drawn using GraphPad Prism 9.5.0 software (San Diego, CA, USA).

2.14. Statistical Analysis

Continuous variables were compared between two groups with paired t test or Wilcoxon signed-rank test. No formal multiple-testing correction was applied to the exploratory comparisons of genomic characteristics and immune cell infiltration estimates. Therefore, the reported p-values for these comparisons are nominal and unadjusted. For gene set enrichment analysis (GSEA), false discovery rate (FDR) q-values were calculated as described in Section 2.12, with an FDR q-value <0.25 considered statistically significant. All tests were performed with GraphPad Prism 9.5.0 software (San Diego, CA, USA). In all analyses, a two-sided or two-tailed p-value below 0.0500 was considered statistically significant.

2.15. Data Availability

The data generated and analyzed during this study are not publicly available to protect patient privacy but are available from the corresponding author upon reasonable request.

3. Results

3.1. Establishment of a Paired Pre/Post-NACT HGSOC Organoid Biobank with Validated Tumor Fidelity

To dissect the biological consequences of NACT in HGSOC, we prospectively established a PDO biobank from gynecologic malignancies treated at the PLA general hospital since 2021. Viable tumor specimens were procured from primary and metastatic lesions, as well as malignant pleural and abdominal serous effusions, with PDOs establishment

achieved within 2–4 weeks. HGSOC-derived PDOs recapitulated parental tumor architecture, manifesting as spheroid structures with papillary fronds and glandular-like protrusions (Figure 1A).

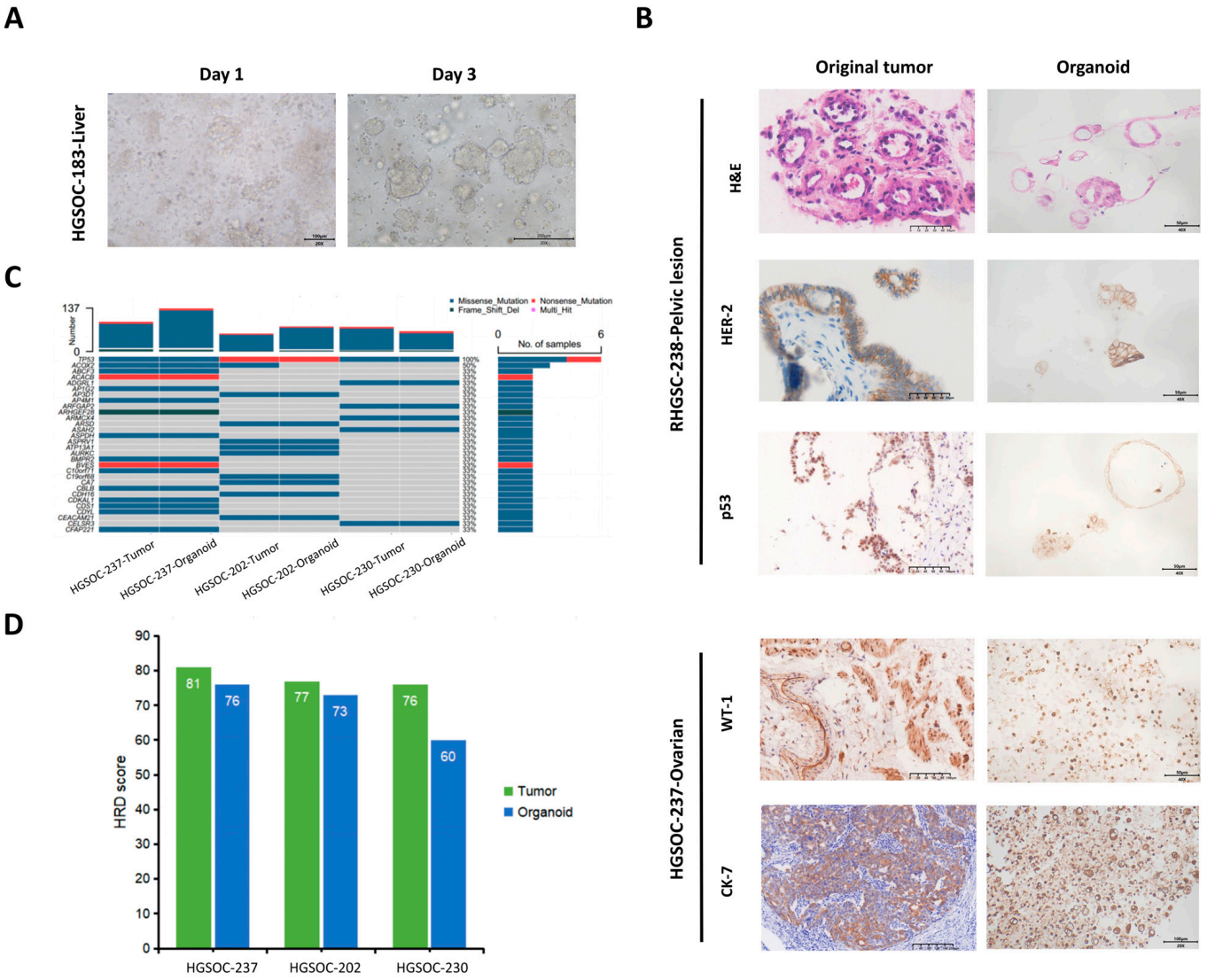


Figure 1. Patient-derived organoids recapitulate the heterogeneity of primary HGSOC tumors. (**A**) Brightfield microscopy images of HGSOC organoids on Day 1 and 3 of culture. (**B**) Representative H&E and IHC staining of original tumor tissues and matched organoids (antibodies as indicated). (**C**) Heatmap of gene mutation frequencies for the most commonly altered genes in HGSOC. (**D**) HRD scores of paired organoids and parental tumor samples' somatic mutations. PDO nomenclature is based on their histopathological subtype followed by patient number. Abbreviations: HGSOC, high-grade serous ovarian carcinoma. RHGSC, recurrent high-grade serous carcinoma.

To rigorously validate the fidelity of our PDO models, we performed paired histological, immunohistochemical, and genomic characterization. Hematoxylin and eosin staining and immunohistochemistry confirmed concordant expression of HGSOC lineage markers—including PAX8, HER2, WT-1, CK7, and p53 patterns—between PDOs and their parental tumors (Figure 1B). WES of three tumor–PDO pairs demonstrated highly concordant somatic mutational profiles, with universal TP53 mutations preserved across all specimens (Figure 1C). In these three paired validation cases, the parental tumors were HRD-positive (score > 42). The PDOs derived from them preserved this HRD-positive status, although modest score reductions were observed (Figure 1D). Gene homology

analysis showed >90% similarity within matched pairs and low interpatient homology, excluding cross-contamination (Supplementary Figure S1).

From this validated biobank, we selected 14 HGSOC patients undergoing NACT-IDS with longitudinal tissue availability, generating 33 matched PDOs from paired pre-NACT and post-IDS samples. The cohort comprised 14 enrolled patients (P1–P14), of which 13 had successful PDO assays (excluding P8), and 11 had paired sequencing data (P1–P11). Primary analyses utilized patient-matched specimens regardless of anatomical site, while confirmatory analyses were restricted to strictly site-matched paired specimens from the same anatomical location. Patient demographics are summarized in Table 1.

3.2. NACT Largely Preserves Tumor Cell-Intrinsic Chemosensitivity in HGSOC

To determine whether NACT alters tumor cell-intrinsic drug responsiveness, we performed chemosensitivity assays on PDOs using guideline-recommended chemotherapeutics and approved PARP inhibitors, including paclitaxel–carboplatin, carboplatin, adriamycin–carboplatin, docetaxel–carboplatin, epirubicin, gemcitabine, etoposide, niraparib, and olaparib. To visualize drug sensitivity changes following NACT, we plotted IC_{50} values of post-NACT PDOs as the vertical coordinate against those of pre-NACT PDOs as the horizontal axis (Figure 2). Each data point represents paired PDOs from the same patient and anatomical site tested with the same drug. The majority of paired data points clustered along the diagonal or within concordant quadrants, indicating that PDO drug sensitivity was largely preserved following NACT exposure.

Given the central role of platinum-based regimens in HGSOC management, we focused on PDOs' responses to carboplatin and paclitaxel–carboplatin (TC) (Supplementary Table S1). To overcome the confounding effect of spatial heterogeneity, we focused on the most stringent subset: six strictly site-matched PDO pairs from four patients with successful assays for the same drug before and after NACT. As shown in Figure 2A,B, apart from PDOs derived from Patient 10's peritoneal and omental metastases—which exhibited mildly elevated TC IC_{50} values that nonetheless remained within the chemosensitive range—all other site-matched PDOs demonstrated reduced or unchanged IC_{50} values following NACT. Statistical analysis of these strictly paired samples confirmed the preservation of tumor cell-intrinsic platinum sensitivity: the mean difference (post-NACT minus pre-NACT) in carboplatin IC_{50} was −3.298 (95% CI: −9.892 to 3.295; $p = 0.2548$), and the mean difference in TC IC_{50} was −0.300 (95% CI: −1.686 to 1.086; $p = 0.6020$), indicating a slight decrease in IC_{50} values following NACT.

To further assess the overall trends across all successfully tested agents, we further performed exploratory analyses. As shown in Figure 2C, the overall IC_{50} changes across all successfully tested agents showed that most paired data points clustered along the diagonal or within concordant quadrants. Because not all site-matched specimens yielded successful assays for the exact same drug, we approximated missing values using available data from homologous primary ovarian tumors from the same patient. As shown in Figure 2D, most PDOs exhibited unchanged sensitivity to carboplatin or paclitaxel–carboplatin. Notably, five cases demonstrated platinum resistance in pre-NACT PDOs but converted to platinum sensitivity in post-NACT PDOs, whereas one case showed the opposite pattern.

Collectively, while acknowledging the limitations of the small sample size and inter-site heterogeneity, these orthogonal functional analyses provide consistent evidence that NACT largely preserves tumor cell-intrinsic platinum sensitivity in HGSOC.

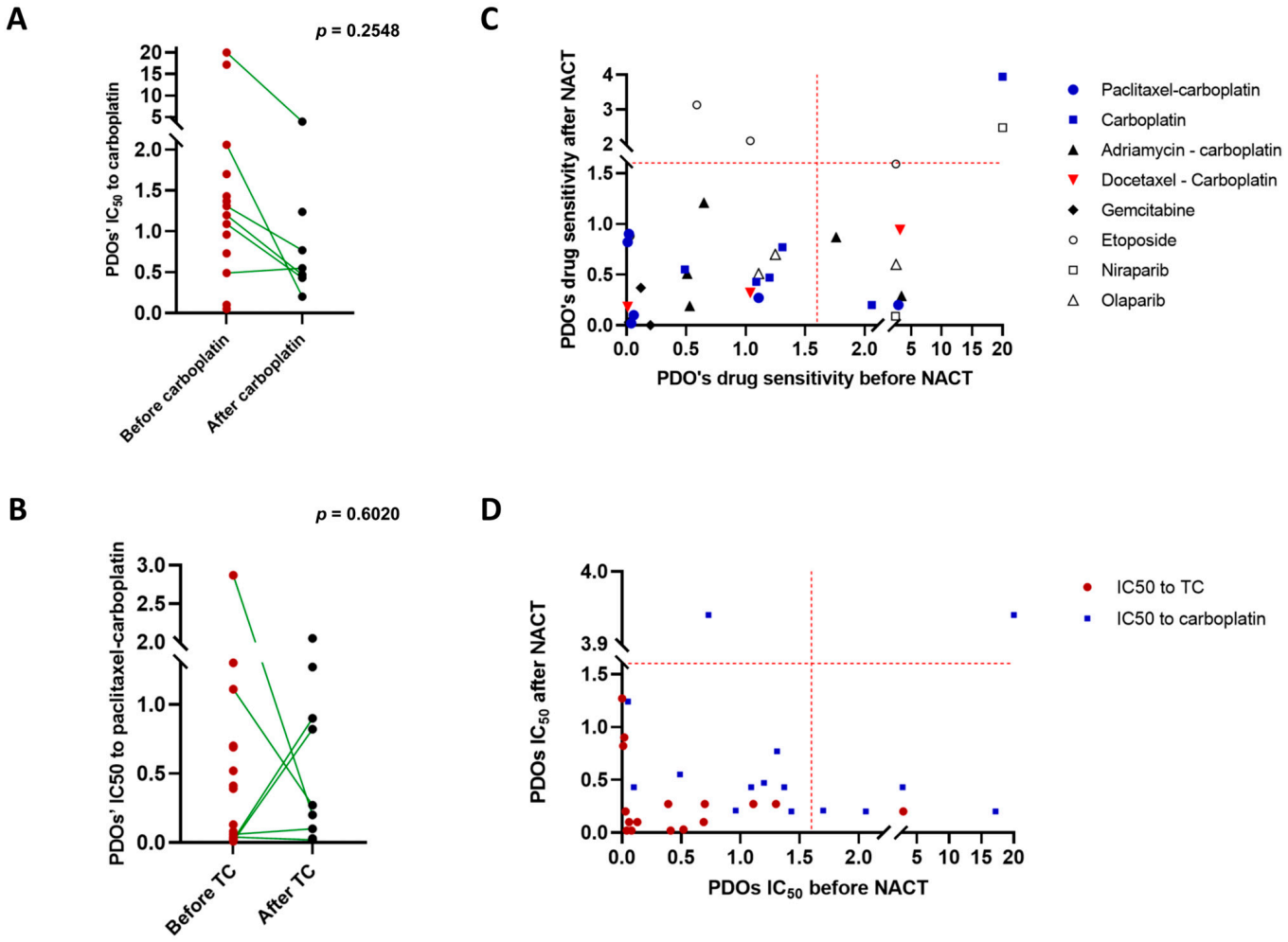


Figure 2. Drug sensitivity of PDOs derived from pre- and post-NACT matched tumors. (**A**,**B**) Drug sensitivity of PDOs to carboplatin (**A**) and paclitaxel–carboplatin (TC) (**B**) derived from strictly site-matched pairs (n = 4 patients, 6 pairs) without any imputation. Individual points with connecting lines represent paired PDOs from the same patient and identical anatomical site. p-values were calculated using paired t-tests. (**C**) Overall IC_{50} changes across all successfully tested agents. This exploratory scatter plot shows the distribution of drug sensitivity for paired homologous lesions of the same patient across various therapeutic regimens. (**D**) Exploratory analysis using imputed missing values from homologous primary ovarian tumors. Scatter plot of drug sensitivity for TC and carboplatin after imputation of missing values to expand the sample size. Abbreviations: PDOs, patient-derived organoids; TC, paclitaxel–carboplatin; NACT, neoadjuvant chemotherapy.

3.3. NACT Does Not Induce Detectable Genomic Evolution in a Limited HGSOC Cohort

Building upon the functional findings, we next interrogated whether NACT induces detectable genomic remodeling. 26 paired samples from 11 patients identified 2648 somatic mutations involving 1608 genes were detected, with a median mutation number of 101 (range 37–186). Consistent with the canonical HGSOC genomic landscape, the most frequently mutated gene was TP53 (76.92%, 20/26). Pathogenic germline BRCA1 mutations were detected in five patients and somatic BRCA2 gene mutation were detected both in pre-NACT and post-NACT samples in one individual (Figure 3A).

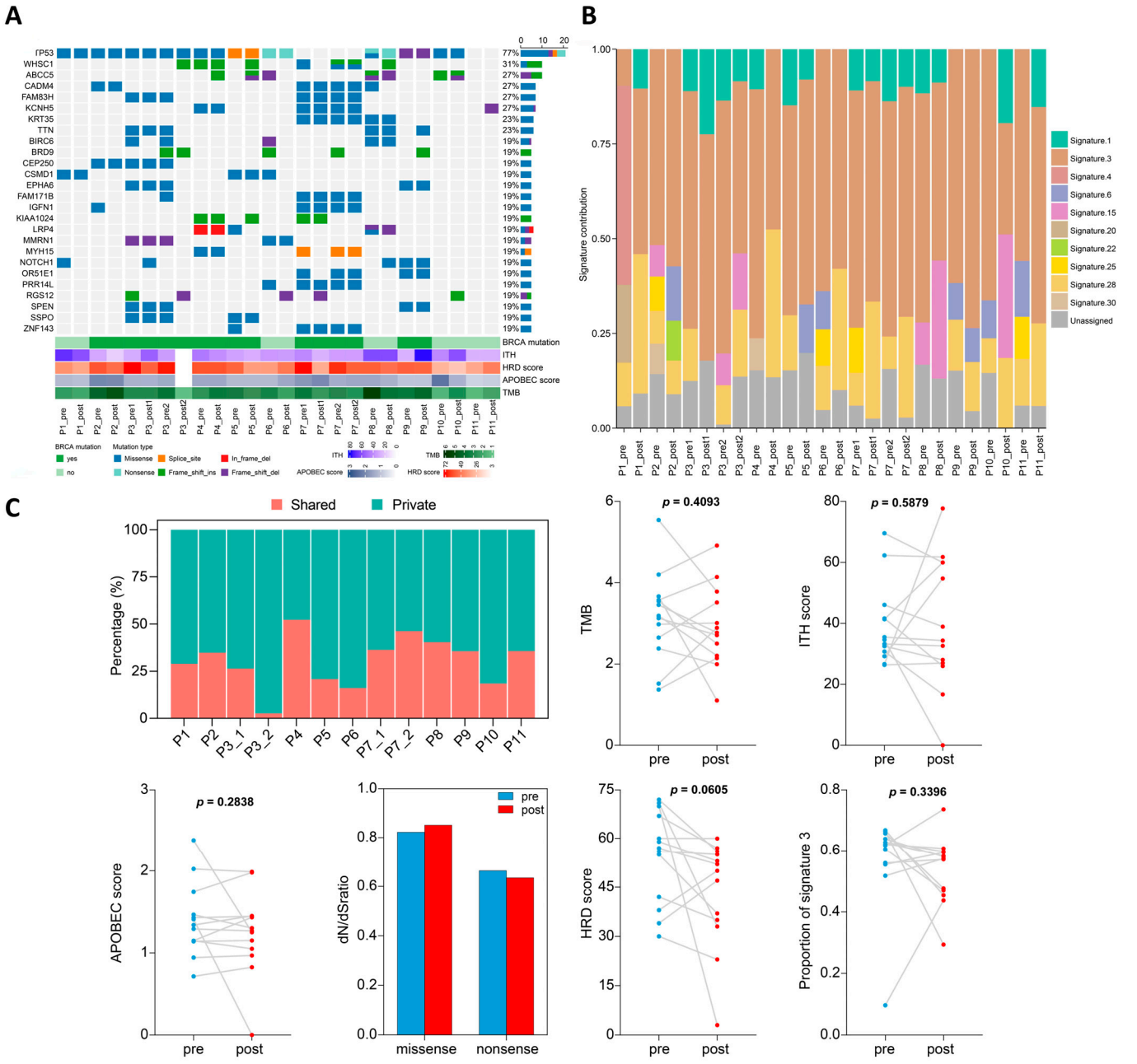


Figure 3. Gene mutational spectrum between pre-NACT and post-NACT tumors. (**A**) Top 26 gene mutations in 26 samples. (**B**) Somatic mutational signature contributions among 26 samples. (**C**) Comparisons of genomic characteristics between pre-NACT and post-NACT tumors. Abbreviations: ITH, intratumoral heterogeneity. HRD, homologous recombination deficiency. APOBEC, apolipoprotein B mRNA-editing enzyme catalytic-polypeptide. TMB, tumor mutational burden.

A substantial proportion of somatic mutations were shared between pre- and post-NACT tumors within individual patients, indicating preservation of the dominant clonal architecture. Mutational signature analysis revealed that Signature 3 (associated with HRD) and Signature 1 (associated with age-related deamination) were the predominant contributors across both pre- and post-NACT specimens, with no significant shift in signature composition following chemotherapy (Figure 3B).

Common somatic variants were observed in pre-NACT and post-NACT tumors for each case. The number of shared somatic mutations ranged from 4–90 (the proportion of shared mutations ranged from 2.56–52.21%). Genomic features were compared and it revealed that no significant differences in TMB (average: 3.17 vs. 2.90, $p = 0.4093$), ITH score (average: 39.21 vs. 39.82, $p = 0.5879$) and APOBEC score (average: 1.40 vs. 1.24, $p = 0.2838$) were observed between pre- and post-NACT tumors (Figure 3C). The dN/dS ratios of missense and nonsense mutations were close between two groups, indicating similar selection in cancer and somatic evolution between pre- and post-NACT tumors. A trend toward decreased HRD scores was observed post-NACT (55 vs. 43, $p = 0.0605$), with a concordant trend in Signature 3 contribution (0.5729 vs. 0.5360, $p = 0.3396$), though neither reached statistical significance. Notably, this decrease in mean HRD score was accompanied by an individual-level transition from HRD-positive to HRD-negative status in several patients (e.g., P1, P5, and P7).

These convergent genomic analyses suggest that short-term NACT exposure in HGSOC largely preserves the genomic landscape of tumor cells. However, given the limited sample size and statistical power to detect subtle genomic changes, we cannot exclude the possibility that other mechanisms, such as epigenetic alterations, contribute to treatment resistance. Additionally, the observed downward trend in HRD scores warrants further investigation.

3.4. NACT Remodels TME Toward an Immunogenic State

Given the apparent genomic and functional stability of tumor cells following NACT, we hypothesized that the biologically relevant impact of NACT might instead manifest within the TME. We therefore characterized immune cell composition in paired pre- and post-NACT specimens using complementary deconvolution algorithms applied to bulk RNA sequencing data.

Transcriptomic pathway analysis revealed significant enrichment of genes involved in NK cell-mediated cytotoxicity, T cell receptor signaling, antigen processing and presentation, and B cell receptor signaling in post-NACT tumors (Figure 4A).

CIBERSORT demonstrated significant enrichment of CD8+ T cells (0.0988 vs. 0.1393, $p = 0.0166$) and activated NK cells (0.0475 vs. 0.0859, $p = 0.0041$) in post-NACT tumors compared to pre-NACT tumors, accompanied by a reduction in monocytes infiltration (0.0454 vs. 0.0268, $p = 0.0297$) (Figure 4B). In addition, CYT score was significantly elevated after NACT treatment (4.5227 vs. 9.7517, $p = 0.0398$) (Figure 4C). These findings were corroborated by MCP-counter analysis, which demonstrated significant post-NACT upregulation of B lineage (4.9774 vs. 16.5523, $p = 0.0215$), CD8+ T cells (1.5713 vs. 5.2941, $p = 0.0266$), cytotoxic lymphocytes (0.9123 vs. 2.3632, $p = 0.0024$), myeloid dendritic cells (1.9400 vs. 3.8247, $p = 0.0327$), and NK cells (0.2342 vs. 0.3299, $p = 0.0398$) were significantly upregulated in post-NACT tumors (Figure 4D).

Collectively, these findings suggest that NACT reshapes the HGSOC microenvironment toward a more immunogenic state, characterized by enhanced cytotoxic effector cell infiltration and coordinated activation of innate and adaptive immune signaling features that may provide a rationale for future combinatorial immunotherapy strategies. However, because these results are based on transcriptomic deconvolution algorithms, they represent estimated cellular composition and require independent validation.

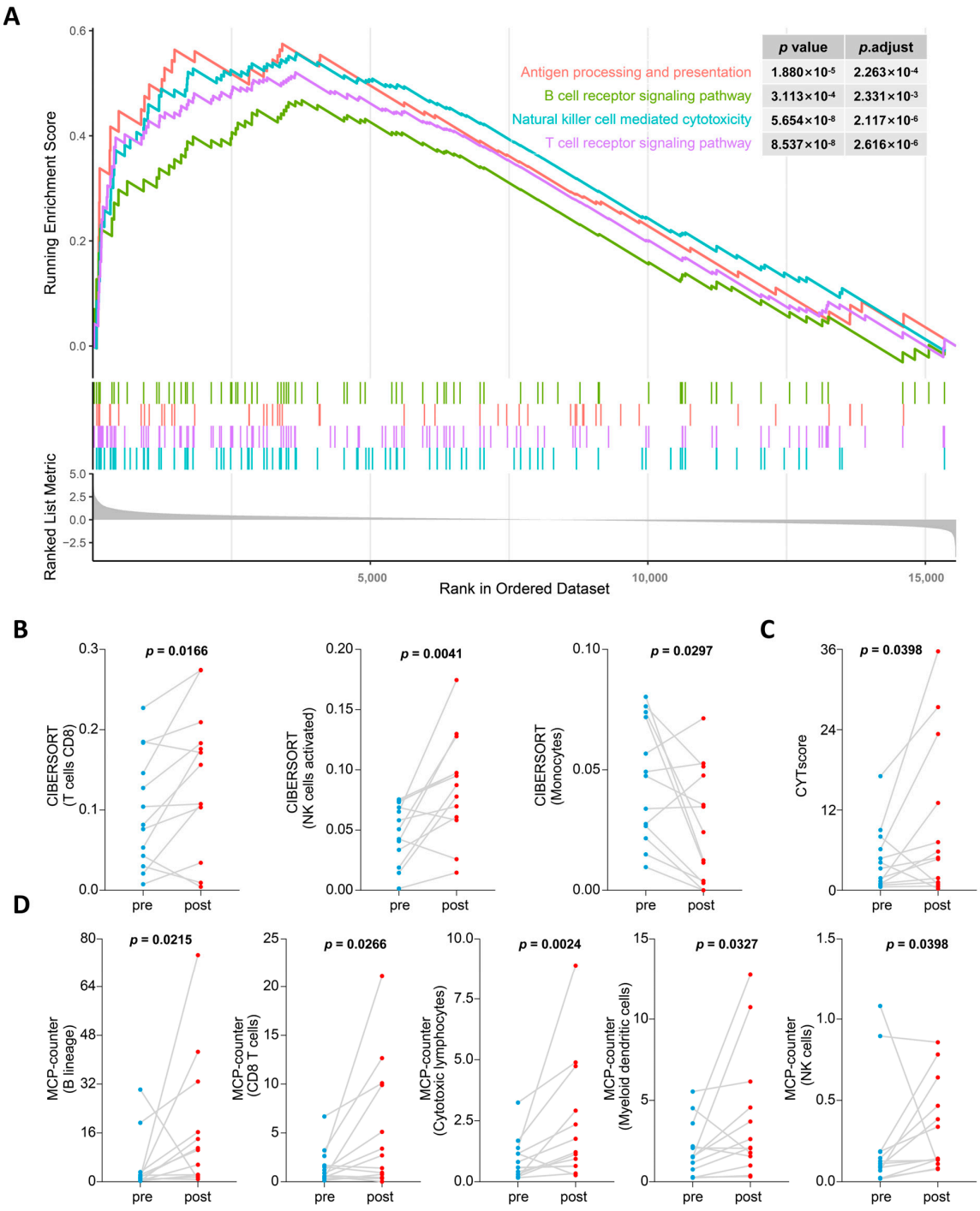


Figure 4. (**A**) Genes involved in immune signaling pathways were significantly enriched in post-NACT tumors. Comparisons of immune cell infiltration between pre-NACT and post-NACT tumors. Immune infiltration estimated by CIBERSORT algorithm (**B**), CYT score (**C**) and MCP-counter algorithm (**D**).

3.5. PDO Drug Sensitivity and Correlation with Clinical Characteristics

To translate our molecular and functional findings into clinically actionable insights, we integrated PDO chemosensitivity data with longitudinal clinical outcomes across the 13-patient cohort. We first assessed drug sensitivity using waterfall plots grouped either by patient (Figure 5A) or by timepoint (pre-NACT vs. post-NACT) (Figure 5B). Substantial intrapatient heterogeneity was observed across PDOs derived from different lesion sites within the same patient, while timepoint-based grouping revealed variable shifts in IC_{50} following neoadjuvant chemotherapy, suggesting that the selective pressure of chemotherapy

may differentially modulate drug sensitivity among individual patients. o integrate PDOs drug sensitivity with clinical characteristics, we generated a heatmap integrating clinical annotations with representative IC_{50} values selected according to a hierarchical priority: PDOs derived from ovarian primary lesions were preferred when available, followed by omentum/peritoneum metastases, and finally ascitic or pleural effusion (Figure 5C). Clinical and treatment features, including age, FIGO stage, CA125 reduction (%), cytoreduction status, bevacizumab combination therapy, treatment response, and patients' platinum sensitivity, were annotated as color-coded bars adjacent to the heatmap. Patients achieving CR or PR tended to have PDOs with lower IC_{50} values, whereas those with platinum-resistant disease or early relapse (within 6 months) tended to have higher IC_{50} values, although the difference was less pronounced than expected.

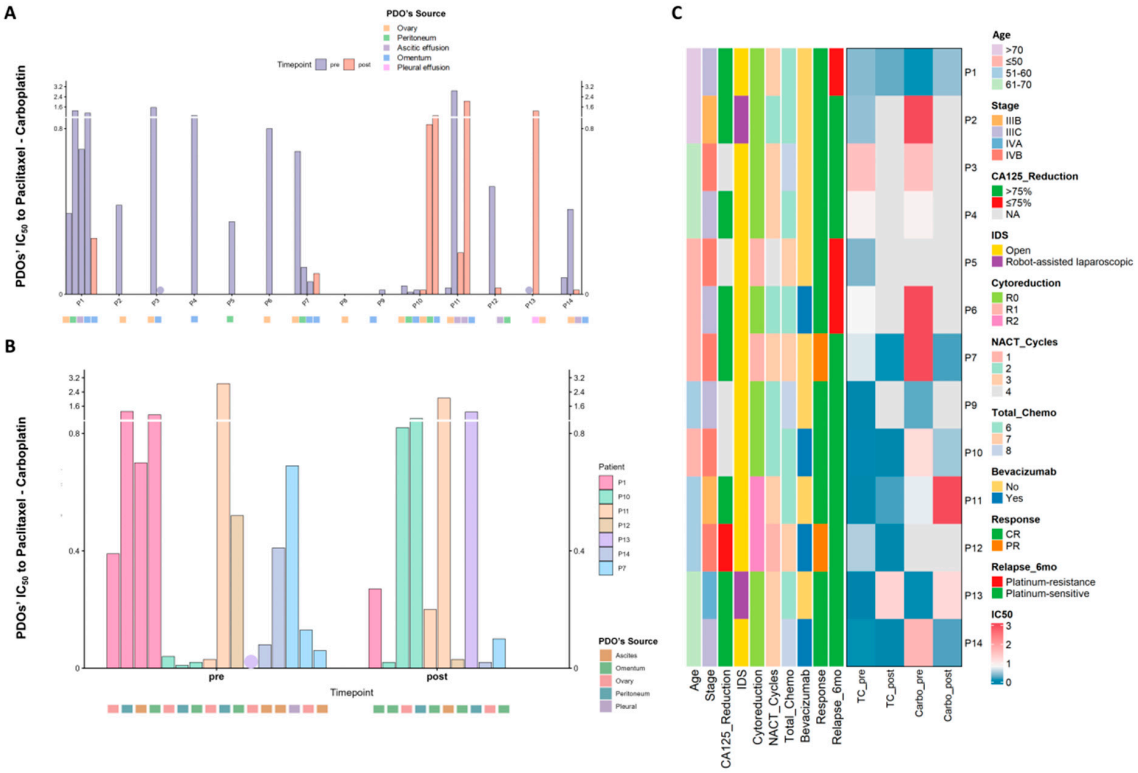


Figure 5. Clinical characteristics and PDOs' drug sensitivity in ovarian cancer patients. (**A**) Patient-grouped waterfall plot of PDOs' IC_{50} values to paclitaxel–carboplatin (TC) regimen. Bars represent individual PDO samples. (**B**) Timepoint-grouped waterfall plot, color-coded by patient for paired pre/post comparison. This figure includes only patients for whom PDOs from both pre- and post-NACT tissues were successfully established and evaluated for sensitivity to TC regimen. (**C**) Heatmap integrating clinical characteristics and representative PDO drug sensitivity for each patient. The heatmap body displays IC_{50} values of PDOs to the TC regimen and carboplatin monotherapy, using a blue-to-red gradient (blue: low IC_{50}, sensitive; red: high IC_{50}, resistant). Left annotation bars summarize patient-level clinical and treatment features, including: Age at the time of tumor sampling and PDO establishment; FIGO stage (IIIA-IVB); CA125 reduction, defined as the percentage decline in serum CA125 level measured before interval debulking surgery (IDS) relative to the pre-NACT baseline; IDS surgical approach (Open vs. Robot-assisted laparoscopic); Cytoreduction status assessed by residual tumor size after IDS: R0, no macroscopic or microscopic residual disease; R1, microscopic residual disease only; R2, macroscopic residual disease; Bevacizumab use as part of adjuvant therapy (yes/no); Treatment response, categorized as complete response (CR), partial response (PR), stable disease (SD), or progressive disease (PD); Relapse_6mo, defined as relapse within 6 months after completion of chemotherapy (platinum-resistant vs. platinum-sensitive). Patients are arranged by ID number (P1–P14) on the y-axis.

To further evaluate the predictive value of PDO-based functional testing, we performed Kaplan–Meier survival analyses for TTP using two complementary baseline selection strategies (Supplementary Figure S2). Using the most-resistant solid lesion prioritization strategy (selecting the highest IC_{50} among all PDOs from solid lesions before NACT as the patient's representative value; $n = 11$, median $IC_{50} = 2.77$), the PDO-sensitive group ($n = 5$) and PDO-resistant group ($n = 6$) had median TTP of 14.10 and 14.80 months, respectively (Hazard Ratio [HR] = 0.944, 95% CI: 0.255–3.504; Log-rank $p = 0.931$, Figure S2A). Similarly, using the primary-site prioritization strategy (selecting the IC_{50} of PDO from the primary ovarian lesion before NACT as the patient's representative value; $n = 13$, median $IC_{50} = 1.2$), the median TTP was 15.35 months for the sensitive group (n = 6) and 15.00 months for the resistant group ($n = 7$) (HR = 1.220, 95% CI: 0.366–4.065; Log-rank $p = 0.740$, Figure S2B). The survival curves for PDO-sensitive and PDO-resistant groups largely overlapped, and no statistically significant difference was observed. This lack of significance is highly likely due to the extremely limited sample size (n = 5–7 per subgroup) and the short follow-up period, which severely restricted the statistical power to detect clinical outcome differences.

Collectively, these integrative exploratory analyses suggest that the combined assessment of PDO functional response and TME immune contexture may provide complementary prognostic information in NACT-treated HGSOC. The preservation of tumor cell-intrinsic chemosensitivity, coupled with TME immune activation, provides a rationale for future investigation into biology-informed chemo-immunotherapy combinations in patients managed with the NACT-IDS approach.

4. Discussion

The present study integrats patient-derived organoids (PDOs) functional assays with paired multi-omics genomic and transcriptomic profiling to investigate the impact of NACT in HGSOC. Our principal findings reveal a dual biological consequence of NACT: preservation of tumor cell-intrinsic chemosensitivity alongside significant remodeling of the tumor microenvironment (TME) toward an immunogenic state. These results suggest a strong rationale for combining NACT with immune checkpoint blockade in future clinical investigations.

In this study, we successfully established PDOs from patient samples, confirmed their histological and genomic fidelity to the original tumors. By profiling IC_{50} values across various agents, we observed that sensitivity to conventional drugs remained largely unchanged in most PDOs. Focusing on clinical regimens (carboplatin and TC), strictly site-matched PDO pairs demonstrated reduced or unchanged IC_{50} values post-NACT, indicating that NACT did not induce acquired chemoresistance in these models. Consistent with previous reports highlighting the predictive value of PDOs in ovarian cancer [32,33], our PDO drug sensitivity screening suggests that these patients did not develop increased chemoresistance after NACT; moreover, NACT largely preserves tumor cell-intrinsic platinum sensitivity.

To further validate this finding, we performed genomic and immunomic bioinformatics analyses on paired HGSOC tumors. As expected, abundant shared gene mutations were detected in both pre- and post-NACT tumors, and no significant differences were observed in tumor mutational burden (TMB), intratumoral heterogeneity (ITH), APOBEC score, homologous recombination deficiency (HRD) score, Signature 3, or dN/dS ratio—findings consistent with previous studies [19,34]. These results indicate that NACT does not induce major genomic perturbations. However, a trend toward a decrease in HRD score in post-NACT tumors approached statistical significance, similar to observations in other studies [35]. This post-NACT reduction in HRD score may be attributable to the fact that HRD-positive tumor cells are more sensitive to chemotherapy [36], leaving residual cells that are predominantly HRD-negative. This hypothesis is further supported by the

individual-level data, where several patients showed a clear transition from HRD-positive to HRD-negative status following NACT. Collectively, while our limited cohort did not detect statistically significant genomic alterations, we cannot exclude the possibility of subtle biological changes. We hypothesize that the downward trend in HRD scores may reflect the selective elimination of HRD-positive cells by chemotherapy. Further studies with larger cohorts are required to validate whether this translates to chemoresistance.

Additionally, changes in the TME during NACT were assessed using RNA-seq data. Post-NACT tumors exhibited significantly higher infiltration of $CD8^+$ T cells, natural killer (NK) cells, activated NK cells, B lineage cells, cytotoxic lymphocytes, and myeloid dendritic cells, as well as higher CYT scores. Furthermore, genes involved in immune signaling pathways—including NK cell-mediated cytotoxicity, T cell receptor signaling, antigen processing and presentation, and B cell receptor signaling—were significantly enriched in post-NACT tumors. Similar findings have been reported previously [34]. Specifically, Alejandro et al. demonstrated increased NK cell infiltration after NACT in HGSOC [37], and Lee et al. found that NACT enhanced tumor-infiltrating lymphocyte (TIL) and CD8+ T cell infiltration, with significant enrichment of immune-related gene sets in post-NACT ovarian tumors [38]. Lodewijk et al. also observed that NACT induced higher TIL abundance and CD8+ T cell infiltration [39]. $CD8^+$ T cells play a pivotal role in anticancer immune responses and form the backbone of cancer immunotherapy [39]. Cytotoxic lymphocytes and NK cells are key effectors in eliminating tumor cells [40]. B cells, as major components of the adaptive immune system, participate in antigen presentation, enhance cytokine-mediated signaling, and secrete tumor-specific antibodies, thereby promoting antitumor immunity [41]. Dendritic cells are professional antigen-presenting cells that bridge innate and adaptive immunity and may play a critical role in antitumor responses. Elevated CYT scores reflect higher immune cytolytic activity associated with $CD8^+$ T cell activation [42]. However, it is important to acknowledge that these findings are based on transcriptomic deconvolution algorithms (CIBERSORT and MCP-counter), which provide indirect estimates of cellular composition. We did not directly assess the functional state of these immune cells or the expression of key exhaustion markers, specifically PD-1, PD-L1, and TIM-3. Therefore, the observed shift toward an immunologically active microenvironment requires further functional validation.

To translate our molecular and functional findings into clinically actionable insights, we integrated PDO chemosensitivity data with longitudinal clinical outcomes. PDO-defined platinum sensitivity showed a trend toward longer time to tumor progression (TTP) compared with the PDO-resistant group, although this did not reach statistical significance due to the limited cohort size. Similarly, patients exhibiting greater post-NACT enhancement of $CD8^+$ T cell infiltration also demonstrated trends toward improved clinical outcomes, suggesting that the degree of NACT-induced immune activation may carry prognostic significance. While limited by the small cohort size, the association between PDO-defined chemosensitivity and clinical outcomes provides exploratory evidence for the potential predictive value of organoid-based functional testing in the NACT-IDS setting. These findings suggest a rationale for future clinical investigation into combining NACT with immune checkpoint blockade, potentially guiding the design of larger prospective trials (e.g., the ongoing NAIVE [43] and NeoPembrOV [44] trials). However, prospective validation is required before integrating PDO-guided stratification into routine clinical practice.

It is crucial to note that our organoid models primarily evaluate tumor cell-intrinsic chemosensitivity in the absence of the full TME. While our genomic data suggest that NACT preserves intrinsic sensitivity, we acknowledge that clinical chemoresistance in HGSOC is multifactorial. Although our transcriptomic analyses revealed dynamic immune changes, our study did not perform functional experiments such as co-culture models to

directly demonstrate that TME components drive clinical resistance. Therefore, the potential dominant role of the TME in clinical chemoresistance remains a hypothesis that warrants further investigation.

Several limitations warrant acknowledgment. First, the relatively small sample size ($n = 13$ for PDOs; $n = 11$ for sequencing) limits statistical power. Specifically, the limited paired sequencing specimens restricted the precision of effect estimation (95% CIs) for TMB, ITH, and HRD; thus, the absence of statistical significance does not exclude relevant biological changes. Second, baseline HRD status was heterogeneous and not a prospective inclusion criterion; the high proportion of HRD-positive cases may represent a selection bias. Additionally, paired specimens were not always from identical anatomical sites; however, the established clonal homogeneity of HGSOC peritoneal disease [45] and our demonstration of >90% intrapatient genomic concordance mitigate this concern. Third, transcriptomic deconvolution (CIBERSORT/MCP-counter) provides indirect estimates. We did not directly assess immune functional states or exhaustion markers (e.g., PD-1, PD-L1, TIM-3), and multiple exploratory comparisons were made without formal multiple-testing correction. Finally, the absence of single-cell resolution and the relatively short follow-up period may underestimate subclonal dynamics and late recurrences, respectively, warranting validation in larger prospective cohorts.

5. Conclusions

In summary, our integrative analysis suggests that NACT largely preserves tumor cell-intrinsic chemosensitivity while reshaping the TME toward an immunogenic state in HGSOC. We hypothesize that the apparent paradox between molecular stability and clinical resistance observations may be partially driven by TME-mediated mechanisms, a concept that warrants direct functional validation in future studies. We propose that the NACT-induced immunogenic window may represent a potential therapeutic opportunity for combinatorial chemo-immunotherapy strategies. Furthermore, PDO-based functional testing shows promise as a potential predictive tool for personalized treatment selection in HGSOC patients; however, its clinical utility requires prospective validation in larger cohorts.

Supplementary Materials: The following supporting information can be downloaded at: https://www.mdpi.com/article/10.3390/life16122037/s1, Table S1: Raw IC_{50} values of PDOs to TC regimen and carboplatin monotherapy, stratified by patient, anatomical site, and treatment timepoint. Figure S1: Homology analysis between organoids and their corresponding original tumors. Figure S2: Kaplan–Meier survival analysis of TTP based on different PDO baseline selection strategies.

Author Contributions: Conceptualization: S.L., Y.M. and M.Y.; Methodology: T.Z., Y.W. (Yawen Wu). and L.Z.; Investigation: T.Z., Y.W. (Yawen Wu) and L.Z.; Supervision: L.L., Z.Y. and X.F.; Formal analysis: Q.Z. and M.L.; Software: Y.W. (Yue Wang), M.W. and N.W.; Data curation: M.C. and X.W.; Resource: S.L., Y.M. and M.Y.; Project administration: S.L., Y.M. and M.Y.; Writing—original draft: T.Z., L.Z. and Y.W. (Yawen Wu); Writing—review and editing: T.Z., L.Z. and M.Y. All authors have read and agreed to the published version of the manuscript.

Funding: This research was funded by the Military Family Planning Independent Research Project, grant No. 26JSZ10, and the Biomedical Innovation and Development Research Project of the China International Science Exchange Foundation, grant No. SWYY2026002158.

Institutional Review Board Statement: This study was conducted in accordance with the ethical principles of the Declaration of Helsinki and approved by the Ethical Committee of Chinese People's Liberation Army General Hospital on the 30th of September 2021 (approval number: S2021-520-01).

Informed Consent Statement: Written informed consent has been obtained from the patients to publish this paper.

Data Availability Statement: The data used to support the findings of this study are available from the corresponding authors upon request.

Acknowledgments: The authors gratefully acknowledge all members who dedicate comprehensive management efforts throughout the treatment of ovarian cancer in our institution. During the preparation of this manuscript, the authors used ChatGPT (GPT-4) for language editing and academic writing assistance. The authors have reviewed and edited the output and take full responsibility for the content of this publication. All scientific content and conclusions were conceived and written by the authors.

Conflicts of Interest: The authors declare no conflicts of interest.

Abbreviations

The following abbreviations are used in this manuscript:

NACT	neoadjuvant chemotherapy
HGSOC	high-grade serous ovarian cancer
IDS	interval debulking surgery
TME	tumor microenvironment
PDOs	patient-derived organoids
WES	whole-exome sequencing
TTP	time to tumor progression
TMB	tumor mutational burden
ITH	intratumoral heterogeneity
APOBEC	apolipoprotein B mRNA-editing enzyme catalytic-polypeptide
HRD	homologous recombination deficiency
NK cells	natural killer cells
EOC	epithelial ovarian cancer
PDS	primary debulking surgery
PARP	Poly (ADP-ribose) polymerase
PLA	People's Liberation Army
H&E	Hematoxylin and eosin
FFPE	formalin-fixed, paraffin-embedded
TC	paclitaxel–carboplatin
hg19	human genome build
SNVs	single nucleotide variants
FDR	false discovery rate

References

1. Caruso, G.; Weroha, S.J.; Cliby, W. Ovarian Cancer: A Review. *JAMA* **2025**, *334*, 1278–1291. [PubMed]
2. Bowtell, D.D.; Böhm, S.; Ahmed, A.A.; Aspuria, P.-J.; Bast, R.C., Jr.; Beral, V.; Berek, J.S.; Birrer, M.J.; Blagden, S.; Bookman, M.A.; et al. Rethinking ovarian cancer II: Reducing mortality from high-grade serous ovarian cancer. *Nat. Rev. Cancer* **2015**, *15*, 668–679. [CrossRef] [PubMed]
3. Torre, L.A.; Bray, F.; Siegel, R.L.; Ferlay, J.; Lortet-Tieulent, J.; Jemal, A. Global cancer statistics, 2012. *CA Cancer J. Clin.* **2015**, *65*, 87–108. [CrossRef] [PubMed]
4. Jacobs, I.J.; Menon, U.; Ryan, A.; Gentry-Maharaj, A.; Burnell, M.; Kalsi, J.K.; Amso, N.N.; Apostolidou, S.; Benjamin, E.; Cruickshank, D.; et al. Ovarian cancer screening and mortality in the UK Collaborative Trial of Ovarian Cancer Screening (UKCTOCS): A randomised controlled trial. *Lancet* **2016**, *387*, 945–956, Correction in *Lancet* **2016**, *387*, 944. [CrossRef] [PubMed]
5. Armstrong, D.K.; Alvarez, R.D.; Bakkum-Gamez, J.N.; Barroilhet, L.; Behbakht, K.; Berchuck, A.; Chen, L.-M.; Cristea, M.; DeRosa, M.; Eisenhauer, E.L.; et al. Ovarian Cancer, Version 2.2020, NCCN Clinical Practice Guidelines in Oncology. *J. Natl. Compr. Cancer Netw. JNCCN* **2021**, *19*, 191–226. [CrossRef] [PubMed]
6. Melamed, A.; Fink, G.; Wright, A.A.; Keating, N.L.; A Gockley, A.; del Carmen, M.G.; O Schorge, J.; Rauh-Hain, J.A. Effect of adoption of neoadjuvant chemotherapy for advanced ovarian cancer on all cause mortality: Quasi-experimental study. *BMJ* **2018**, *360*, j5463. [CrossRef] [PubMed]
7. Vergote, I.; Tropé, C.G.; Amant, F.; Kristensen, G.B.; Ehlen, T.; Johnson, N.; Verheijen, R.H.M.; van der Burg, M.E.L.; Lacave, A.J.; Panici, P.B.; et al. Neoadjuvant chemotherapy or primary surgery in stage IIIC or IV ovarian cancer. *N. Engl. J. Med.* **2010**, *363*, 943–953. [CrossRef] [PubMed]

8. Shawky, M.; Choudhary, C.; Coleridge, S.L.; Bryant, A.; Morrison, J. Neoadjuvant chemotherapy before surgery versus surgery followed by chemotherapy for initial treatment in advanced epithelial ovarian cancer. *Cochrane Database Syst. Rev.* **2025**, *2*, CD5343. [CrossRef] [PubMed]
9. Goff, B.A. Advanced ovarian cancer: What should be the standard of care? *J. Gynecol. Oncol.* **2013**, *24*, 83–91. [CrossRef] [PubMed]
10. Vergote, I.; Coens, C.; Nankivell, M.; Kristensen, G.B.; Parmar, M.K.B.; Ehlen, T.; Jayson, G.C.; Johnson, N.; Swart, A.M.; Verheijen, R.; et al. Neoadjuvant chemotherapy versus debulking surgery in advanced tubo-ovarian cancers: Pooled analysis of individual patient data from the EORTC 55971 and CHORUS trials. *Lancet. Oncol.* **2018**, *19*, 1680–1687, Correction in *Lancet. Oncol.* **2018**, *20*, E10. [CrossRef] [PubMed]
11. Frezzini, S.; Lonardi, S. Spotlight on New Hallmarks of Drug-Resistance towards Personalized Care for Epithelial Ovarian Cancer. *Cells* **2024**, *13*, 611. [CrossRef] [PubMed]
12. Garziera, M.; Cecchin, E.; Giorda, G.; Sorio, R.; Scalone, S.; De Mattia, E.; Roncato, R.; Gagno, S.; Poletto, E.; Romanato, L.; et al. Clonal Evolution of TP53 c.375+1G>A Mutation in Pre- and Post- Neo-Adjuvant Chemotherapy (NACT) Tumor Samples in High-Grade Serous Ovarian Cancer (HGSOC). *Cells* **2019**, *8*, 1186. [CrossRef] [PubMed]
13. Zhang, G.; Liu, H.; Huang, J.; Wang, L.; Zhao, J.-S.; Li, C.; Mi, K.; Zhu, Y.; Cheng, J.; Zha, X. TP53 K351N mutation-associated platinum resistance after neoadjuvant chemotherapy in patients with advanced ovarian cancer. *Gynecol. Oncol.* **2014**, *132*, 752–757. [CrossRef] [PubMed]
14. Gorodnova, T.V.; Sokolenko, A.P.; Ivantsov, A.O.; Iyevleva, A.G.; Suspitsin, E.N.; Aleksakhina, S.N.; Yanus, G.A.; Togo, A.V.; Maximov, S.Y.; Imyanitov, E.N. High response rates to neoadjuvant platinum-based therapy in ovarian cancer patients carrying germ-line BRCA mutation. *Cancer Lett.* **2015**, *369*, 363–367. [CrossRef] [PubMed]
15. Sokolenko, A.P.; Savonevich, E.L.; Ivantsov, A.O.; Raskin, G.A.; Kuligina, E.S.; Gorodnova, T.V.; Preobrazhenskaya, E.V.; Kleshchov, M.A.; Tiurin, V.I.; Mukhina, M.S.; et al. Rapid selection of BRCA1-proficient tumor cells during neoadjuvant therapy for ovarian cancer in BRCA1 mutation carriers. *Cancer Lett.* **2017**, *397*, 127–132. [CrossRef] [PubMed]
16. Pikkusaari, S.; Tumiati, M.; Virtanen, A.; Oikkonen, J.; Li, Y.; Perez-Villatoro, F.; Muranen, T.; Salko, M.; Huhtinen, K.; Kanerva, A.; et al. Functional Homologous Recombination Assay on FFPE Specimens of Advanced High-Grade Serous Ovarian Cancer Predicts Clinical Outcomes. *Clin. Cancer Res. An. Off. J. Am. Assoc. Cancer Res.* **2023**, *29*, 3110–3123. [CrossRef] [PubMed]
17. Kessous, R.; Laskov, I.; Abitbol, J.; Bitharas, J.; Yasmeen, A.; Salvador, S.; Lau, S.; Gotlieb, W.H. Clinical outcome of neoadjuvant chemotherapy for advanced ovarian cancer. *Gynecol. Oncol.* **2017**, *144*, 474–479. [CrossRef] [PubMed]
18. Rauh-Hain, J.A.; Nitschmann, C.C.; Worley, M.J.J.; Bradford, L.S.; Berkowitz, R.S.; Schorge, J.O.; Campos, S.M.; del Carmen, M.G.; Horowitz, N.S. Platinum resistance after neoadjuvant chemotherapy compared to primary surgery in patients with advanced epithelial ovarian carcinoma. *Gynecol. Oncol.* **2013**, *129*, 63–68. [CrossRef] [PubMed]
19. Marchocki, Z.; Tone, A.; Virtanen, C.; de Borja, R.; Clarke, B.; Brown, T.; May, T. Impact of neoadjuvant chemotherapy on somatic mutation status in high-grade serous ovarian carcinoma. *J. Ovarian Res.* **2022**, *15*, 50. [CrossRef] [PubMed]
20. Ben-David, U.; Siranosian, B.; Ha, G.; Tang, H.; Oren, Y.; Hinohara, K.; Strathdee, C.A.; Dempster, J.; Lyons, N.J.; Burns, R.; et al. Genetic and transcriptional evolution alters cancer cell line drug response. *Nature* **2018**, *560*, 325–330. [CrossRef] [PubMed]
21. Senkowski, W.; Gall-Mas, L.; Falco, M.M.; Li, Y.; Lavikka, K.; Kriegbaum, M.C.; Oikkonen, J.; Bulanova, D.; Pietras, E.J.; Voßgröne, K.; et al. A platform for efficient establishment and drug-response profiling of high-grade serous ovarian cancer organoids. *Dev. Cell* **2023**, *58*, 1106–1121. [CrossRef] [PubMed]
22. Hill, S.J.; Decker, B.; Roberts, E.A.; Horowitz, N.S.; Muto, M.G.; Worley, M.J.; Feltmate, C.M.; Nucci, M.R.; Swisher, E.M.; Nguyen, H.; et al. Prediction of DNA Repair Inhibitor Response in Short-Term Patient-Derived Ovarian Cancer Organoids. *Cancer Discov.* **2018**, *8*, 1404–1421. [CrossRef] [PubMed]
23. Ye, M.; Wu, Y.; Chen, Z.; Zhai, Q.; Li, L.; Yan, Z.; Li, M.; Gu, C.; Yang, W.; Liao, S.; et al. Patient-derived ovarian cancer organoids as platforms for predicting platinum resistance and screening tumor stem cell inhibitors. *Drug Resist. Updates Rev. Comment. Antimicrob. Anticancer Chemother.* **2026**, *87*, 101411. [CrossRef] [PubMed]
24. Roberts, S.A.; Lawrence, M.S.; Klimczak, L.J.; Grimm, S.A.; Fargo, D.; Stojanov, P.; Kiezun, A.; Kryukov, G.V.; Carter, C.L.; Saksena, G.; et al. An APOBEC cytidine deaminase mutagenesis pattern is widespread in human cancers. *Nat. Genet.* **2013**, *45*, 970–976. [CrossRef] [PubMed]
25. Martincorena, I.; Raine, K.M.; Gerstung, M.; Dawson, K.J.; Haase, K.; Van Loo, P.; Davies, H.; Stratton, M.R.; Campbell, P.J. Universal Patterns of Selection in Cancer and Somatic Tissues. *Cell* **2018**, *173*, 1823. [CrossRef] [PubMed]
26. Mroz, E.A.; Rocco, J.W. MATH, a novel measure of intratumor genetic heterogeneity, is high in poor-outcome classes of head and neck squamous cell carcinoma. *Oral Oncol.* **2013**, *49*, 211–215. [CrossRef] [PubMed]
27. Sztupinszki, Z.; Diossy, M.; Krzystanek, M.; Reiniger, L.; Csabai, I.; Favero, F.; Birkbak, N.J.; Eklund, A.C.; Syed, A.; Szallasi, Z. Migrating the SNP array-based homologous recombination deficiency measures to next generation sequencing data of breast cancer. *npj Breast Cancer* **2018**, *4*, 16. [CrossRef] [PubMed]

28. Rosenthal, R.; McGranahan, N.; Herrero, J.; Taylor, B.S.; Swanton, C. DeconstructSigs: Delineating mutational processes in single tumors distinguishes DNA repair deficiencies and patterns of carcinoma evolution. *Genome Biol.* **2016**, *17*, 31. [CrossRef] [PubMed]
29. Newman, A.M.; Liu, C.L.; Green, M.R.; Gentles, A.J.; Feng, W.; Xu, Y.; Hoang, C.D.; Diehn, M.; Alizadeh, A.A. Robust enumeration of cell subsets from tissue expression profiles. *Nat. Methods* **2015**, *12*, 453–457. [CrossRef] [PubMed]
30. Becht, E.; Giraldo, N.A.; Lacroix, L.; Buttard, B.; Elarouci, N.; Petitprez, F.; Selves, J.; Laurent-Puig, P.; Sautes-Fridman, C.; Fridman, W.H.; et al. Estimating the population abundance of tissue-infiltrating immune and stromal cell populations using gene expression. *Genome Biol.* **2016**, *17*, 218, Erratum in *Genome Biol.* **2016**, *17*, 249. [CrossRef] [PubMed]
31. Rooney, M.S.; Shukla, S.A.; Wu, C.J.; Getz, G.; Hacohen, N. Molecular and genetic properties of tumors associated with local immune cytolytic activity. *Cell* **2015**, *160*, 48–61. [CrossRef] [PubMed]
32. Weeber, F.; Ooft, S.N.; Dijkstra, K.K.; Voest, E.E. Tumor Organoids as a Pre-clinical Cancer Model for Drug Discovery. *Cell Chem. Biol.* **2017**, *24*, 1092–1100. [CrossRef] [PubMed]
33. Ito, Y.; Kondo, J.; Masuda, M.; Matsuzaki, S.; Onuma, K.; Kanda, M.; Watanabe, Y.; Sakaguchi, H.; Yoshino, K.; Ueda, Y.; et al. Ex vivo chemosensitivity assay using primary ovarian cancer organoids for predicting clinical response and screening effective drugs. *Hum. Cell* **2023**, *36*, 752–761. [CrossRef] [PubMed]
34. Lodewijk, I.; Bernardini, A.; Suárez-Cabrera, C.; Bernal, E.; Sánchez, R.; Garcia, J.L.; Rojas, K.; Morales, L.; Wang, S.; Han, X.; et al. Genomic landscape and immune-related gene expression profiling of epithelial ovarian cancer after neoadjuvant chemotherapy. *npj Precis. Oncol.* **2022**, *6*, 7. [CrossRef] [PubMed]
35. Takaya, H.; Nakai, H.; Sakai, K.; Nishio, K.; Murakami, K.; Mandai, M.; Matsumura, N. Intratumor heterogeneity and homologous recombination deficiency of high-grade serous ovarian cancer are associated with prognosis and molecular subtype and change in treatment course. *Gynecol. Oncol.* **2020**, *156*, 415–422. [CrossRef] [PubMed]
36. Stronach, E.A.; Paul, J.; Timms, K.M.; Hughes, E.; Brown, K.; Neff, C.; Perry, M.; Gutin, A.; El-Bahrawy, M.; Steel, J.H.; et al. Biomarker Assessment of HR Deficiency, Tumor BRCA1/2 Mutations, and CCNE1 Copy Number in Ovarian Cancer: Associations with Clinical Outcome Following Platinum Monotherapy. *Mol. Cancer Res. MCR* **2018**, *16*, 1103–1111. [CrossRef] [PubMed]
37. Jiménez-Sánchez, A.; Cybulska, P.; Mager, K.L.; Koplev, S.; Cast, O.; Couturier, D.-L.; Memon, D.; Selenica, P.; Nikolovski, I.; Mazaheri, Y.; et al. Unraveling tumor-immune heterogeneity in advanced ovarian cancer uncovers immunogenic effect of chemotherapy. *Nat. Genet.* **2020**, *52*, 582–593. [CrossRef] [PubMed]
38. Lee, Y.J.; Woo, H.Y.; Kim, Y.; Park, J.; Nam, E.J.; Kim, S.W.; Kim, S.; Kim, Y.T.; Park, E.; Joung, J.-G.; et al. Dynamics of the Tumor Immune Microenvironment during Neoadjuvant Chemotherapy of High-Grade Serous Ovarian Cancer. *Cancers* **2022**, *14*, 2308. [CrossRef] [PubMed]
39. Raskov, H.; Orhan, A.; Christensen, J.P.; Gögenur, I. Cytotoxic $CD8^+$ T cells in cancer and cancer immunotherapy. *Br. J. Cancer* **2021**, *124*, 359–367. [CrossRef] [PubMed]
40. Le, D.T.; Huynh, T.R.; Burt, B.; Van Buren, G.; Abeynaike, S.A.; Zalfa, C.; Nikzad, R.; Kheradmand, F.; Tyner, J.J.; Paust, S. Natural killer cells and cytotoxic T lymphocytes are required to clear solid tumor in a patient-derived xenograft. *JCI Insight* **2021**, *6*, e140116. [CrossRef] [PubMed]
41. Sharonov, G.V.; Serebrovskaya, E.O.; Yuzhakova, D.V.; Britanova, O.V.; Chudakov, D.M. B cells, plasma cells and antibody repertoires in the tumour microenvironment. *Nat. Rev. Immunol.* **2020**, *20*, 294–307. [CrossRef] [PubMed]
42. Gao, Z.; Zhang, N.; An, B.; Li, D.; Fang, Z.; Xu, D. Comprehensive analyses of the cancer-associated fibroblast subtypes and their score system for prediction of outcomes and immunosuppressive microenvironment in prostate cancer. *Cancer Cell Int.* **2024**, *24*, 127. [CrossRef] [PubMed]
43. Zhang, Z.; Fei, J.; Lao, S.; Liu, R.; Zhu, X.; Zhai, L.; Huang, D.; Deng, B.; Wang, J.; Fang, H.; et al. Neoadjuvant tislelizumab (anti-PD-1 antibody) plus chemotherapy in patients with advanced epithelial ovarian cancer: The exploratory NAIVE trial. *Signal Transduct. Target. Ther.* **2026**, *11*, 265. [CrossRef] [PubMed]
44. Ray-Coquard, I.L.; Savoye, A.; Schiffler, C.; Mouret-Reynier, M.-A.; Derbel, O.; Kalbacher, E.; LeHeurteur, M.; Martinez, A.; Cornila, C.; Martinez, M.; et al. Neoadjuvant and adjuvant pembrolizumab in advanced high-grade serous carcinoma: The randomized phase II NeoPembrOV clinical trial. *Nat. Commun.* **2024**, *15*, 5931. [CrossRef] [PubMed]
45. McPherson, A.; Roth, A.; Laks, E.; Masud, T.; Bashashati, A.; Zhang, A.W.; Ha, G.; Biele, J.; Yap, D.; Wan, A.; et al. Divergent modes of clonal spread and intraperitoneal mixing in high-grade serous ovarian cancer. *Nat. Genet.* **2016**, *48*, 758–767. [CrossRef] [PubMed]

Disclaimer/Publisher's Note: The statements, opinions and data contained in all publications are solely those of the individual author(s) and contributor(s) and not of MDPI and/or the editor(s). MDPI and/or the editor(s) disclaim responsibility for any injury to people or property resulting from any ideas, methods, instructions or products referred to in the content.